Quantitative morphology of a fringing reef tract from high-resolution laser bathymetry: Southern Molokai, Hawaii

C.D. Storlazzi[†]
J.B. Logan[‡]
M.E. Field[§]
U.S. Geological Survey, Pacific Science Center, 1156 High Street, Santa Cruz, California 95064-1077, USA

ABSTRACT

High-resolution Scanning Hydrographic Operational Airborne Lidar Survey (SHOALS) laser-determined bathymetric data were used to define the morphology of spur-and-groove structures on the fringing reef off the south coast of Molokai, Hawaii. These data provide a basis for mapping and analyzing morphology of the reef with a level of precision and spatial coverage never before attained. An extensive fringing coral reef stretches along the central two-thirds of Molokai's south shore (~40 km); along the east and west ends there is only a thin veneer of living coral with no developed reef complex. In total, ~4800 measurements of spur-and-groove height and the distance between adjacent spur crests (wavelength) were obtained along four isobaths. Between the 5m and 15m isobaths, the mean spur height increased from 0.7 m to 1.6 m, whereas the mean wavelength increased from 71 m to 104 m. Reef flat width was found to exponentially decrease with increasing wave energy. Overall, mean spur-and-groove height and wavelength were shown to be inversely proportional to wave energy. In high-energy environments, spur-and-groove morphology remains relatively constant across all water depths. In low-energy environments, however, spur-and-groove structures display much greater variation; they are relatively small and narrow in shallow depths and develop into much larger and broader features in deeper water. Therefore, it appears that waves exert a primary control on both the small- and large-scale morphology of the reef off south Molokai.

Keywords: Fringing reef, reef morphology, spur-and-groove structure, lidar, bathymetry, waves.

INTRODUCTION

Ever since sailors started mapping the approaches to natural harbors at low latitudes, the complex morphology of coral reefs has been evident. Whereas the reef crest was the most important feature for sailors to map due to its shallow depth and obvious hazard to navigation, it was clear that the majority of the reef lay seaward of the reef crest in depths >40 m. Emery et al. (1949) and Munk and Sargent (1954) were some of the first to document and make rough quantitative observations of reef morphology in the western Pacific Ocean. One of the prominent features they documented were elevated shore-normal ridges of coral (coral ''spurs'') seaward of the reef crest that were separated by shore-normal patches of sand (sand ''grooves''). Since then, these features have been termed ''spur-and-groove'' structures and have been observed along reefs elsewhere in the Pacific Ocean (Cloud, 1959; Kan et al., 1997), the Atlantic Ocean (Shinn et al., 1977, 1981), the Indian Ocean (Weydert, 1979), the Caribbean Sea (Goreau, 1959; Roberts, 1974; Geister, 1977; Roberts et al., 1980; Blanchon and Jones, 1995, 1997), and the Red Sea (Sneh and Friedman, 1980).

There has been debate about the origin of these features, from sediment-induced abrasion to preferential constructional growth (i.e., Cloud, 1959; Goreau, 1959; Shinn, 1963; Weydert, 1979; Shinn et al., 1981; Kan et al., 1997). Almost all of the studies on spur-and-groove structures have been based on relatively qualitative data, and the quantitative data that exist are typically very limited in resolution and spatial extent. Past techniques used to describe reefs as a whole, and spur-and-groove structures in particular, have included swim and scuba surveys, aerial photographs, and ship-borne fathometer surveys (i.e., Roberts, 1974; Roberts et al., 1980; Blanchon and Jones, 1995). These methods, which are effective for small areas or when high-resolution data are not available, cannot be used to effectively map large reefs with the precision necessary for quantitative morphologic studies.

The fringing reef off the south coast of Molokai, Hawaii, is currently being studied as part of a U.S. Geological Survey (USGS) multidisciplinary project that focuses on the geologic processes that affect coral reef systems. As part of this study, high-resolution Scanning Hydrographic Operational Airborne Lidar Survey (SHOALS) laser-determined bathymetric data were utilized to help map the reef accurately and analyze its morphology with a level of precision and spatial coverage not previously attained. By combining the SHOALS bathymetric data with field surveys and previously collected low-resolution bathymetry, we were able to: (a) determine the large-scale three-dimensional reef morphology; (b) accurately quantify variations in the height and wavelength of spur-and-groove structures along 40 km of reef; (c) evaluate how spur-and-groove morphology evolves cross-shore from the reef crest to the base of the reef; (d) describe the interrelationships between spur-and-groove morphology and wave energy; and (e) use the data from (a-d) to provide insight into the primary controls on the development of reef complexes and spur-and-groove structures.

[†]E-mail: cstorlazzi@usgs.gov.
[‡]E-mail: jlogan@usgs.gov.
[§]E-mail: mfield@usgs.gov.

GSA Bulletin; November 2003; v. 115; no. 11; p. 1344–1355; 13 figures.

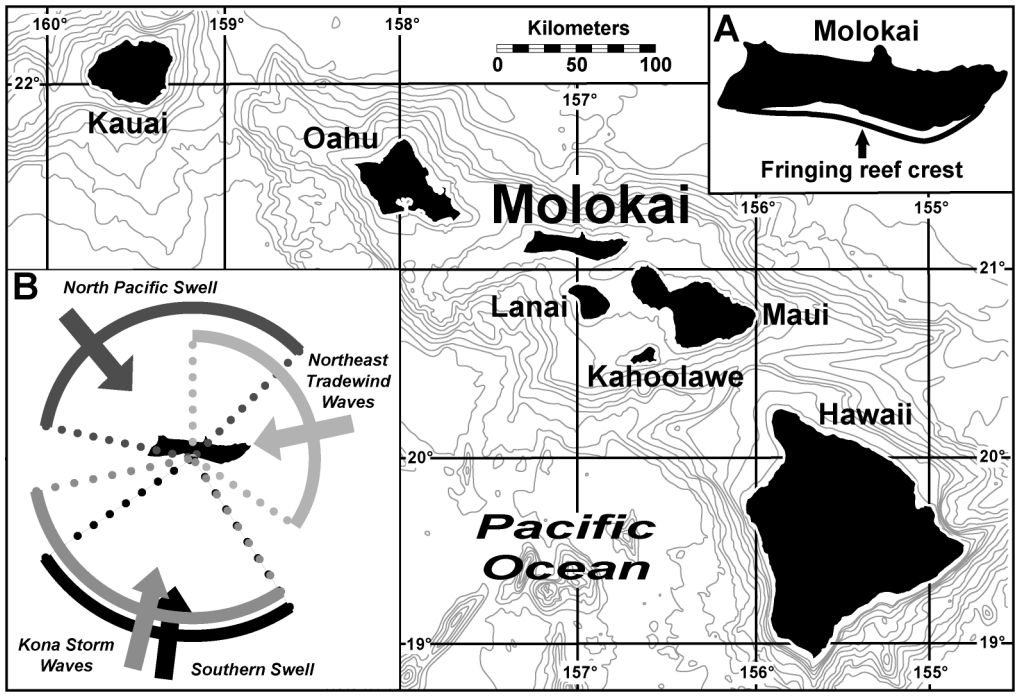

Figure 1. Map of Hawaii's seven main islands, showing the location of Molokai relative to the rest of the main islands. Isobaths are every 100 m from shoreline to 1000 m, below which the isobaths are every 1000 m. (A) Location of the fringing reef crest off the island's south shore. (B) Wave climate for the Hawaiian Islands showing the dominant wave energy end members; modified after Moberly and Chaimberlain (1964).

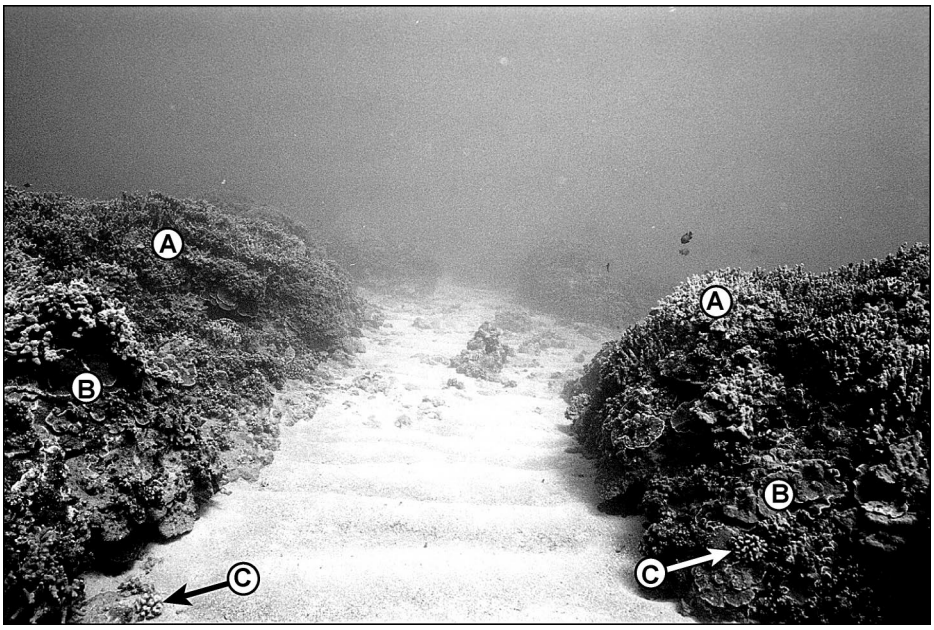

Figure 2. Underwater photograph of a spur-and-groove (SAG) structure off Umipaa (see Fig. 4 for location). The height between the sand-floored groove and the top of the spurs in the photograph is ~1.5 m; the width of the groove is ~2 m. Three of the main reef-building corals can be identified: (A) *Porites compressa* (vertical fingers), (B) *Montipora capitata* (horizontal plates), and (C) *Pocillapora meandrina* (cauliflower). Wave-generated symmetrical ripples cover the sand bed. View is seaward.

STUDY AREA

Location and Geology

The island of Molokai is located ~21°N, 157°W in the North-Central Pacific between the islands of Oahu and Maui in the Hawaiian archipelago (Fig. 1). The island is 62 km long east-west and on average 13 km wide north-south. The island is comprised of two basaltic shield volcanoes formed ~1.90–1.76 m.y.a. (Clague and Dalrymple, 1989); the east Molokai volcano is 1515 m high and the west Molokai volcano is 420 m high.

Oceanography and Meteorology

The wave climate off Molokai can be characterized by four end members: North Pacific swell, northeast trade wind waves, Southern Ocean swell, and Kona storm waves (Moberly and Chaimberlain, 1964). The North Pacific swell is generated by strong winter (November–March) storms as they track from west to east across the North Pacific and have significant wave heights (H_s) of ~3–8 m and peak periods (T_p) of ~10–20 s. The northeast trade wind waves occur throughout the year but are largest from April through November when the trade winds blow the strongest; these

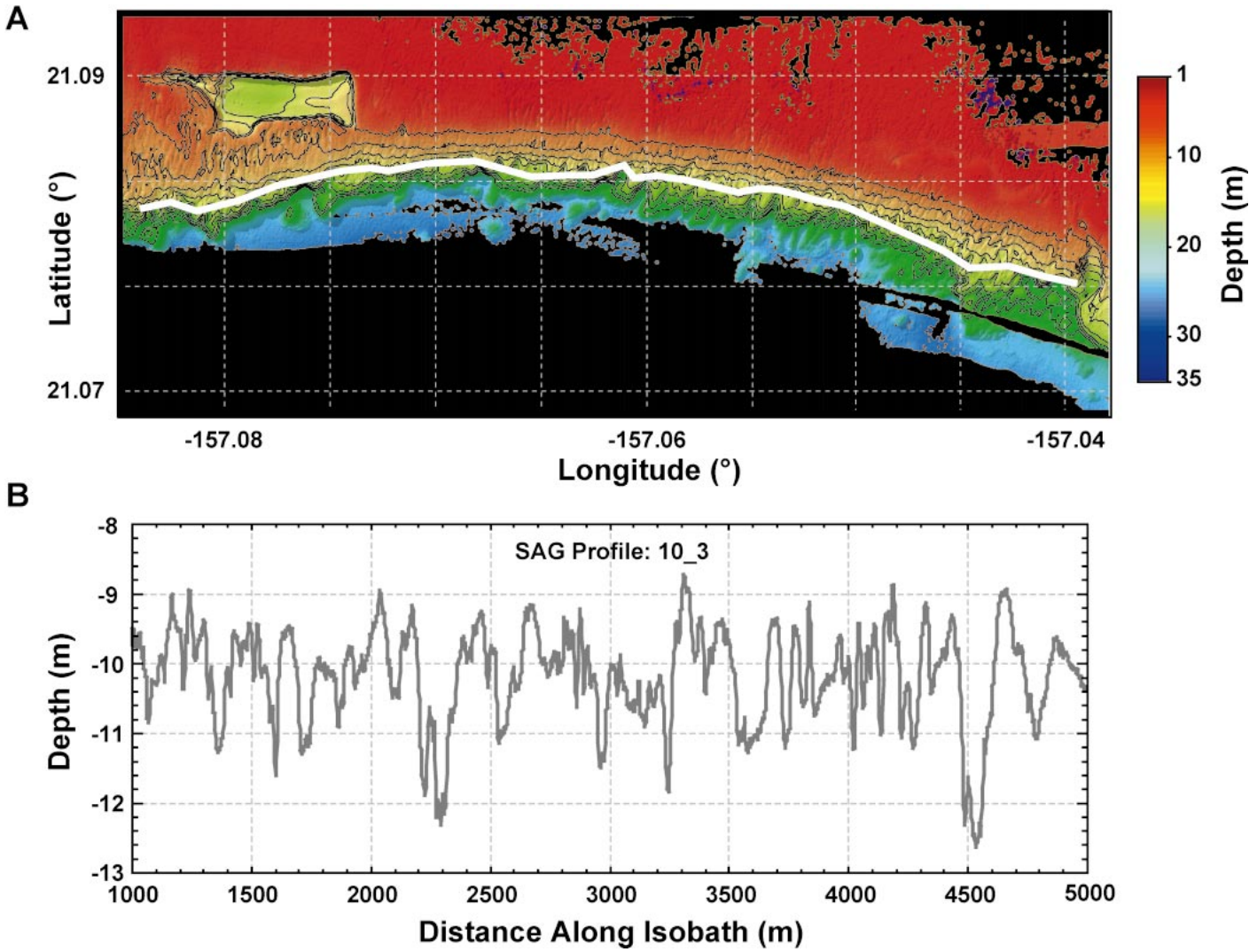

Figure 3. Example of SHOALS lidar bathymetric data. (A) Shaded relief map view of the SHOALS lidar bathymetry overlaid with 2 m contours. Note the roughly shore-normal spur-and-groove (SAG) features. (B) Example of a shore-parallel bathymetric profile along the 10 m isobath. The location of this profile line is the bold white line in Figure 3A.

waves have H_s of ~1–4 m but have very short periods, with T_p of ~5–8 s. The Southern Ocean swell is generated by storms in the Southern Ocean during the Southern Hemisphere winter, and whereas they are typically small (H_s of ~1–2 m), they have very long periods (T_p of ~14–25 s). Kona storm waves occur when local fronts or extra-tropical lows pass through the region, although they are infrequent and inconsistent in their occurrence. Kona storm waves typically have H_s of ~3–4 m and T_p of ~8–12 s.

Precipitation patterns on the island are primarily controlled by two of the four storm patterns listed above: the northeast trade winds and Kona storms. The northeast trade winds primarily strike the northeast side of the island. Due to orographic effects associated with the >1500 m east Molokai shield volcano, most of the precipitation (200–400 cm/yr) falls on this section of the island. Most of the south-central and the entire west side of Molokai receive less than 60 cm/yr on average (State of Hawaii, 2001).

Molokai Reef Tract

A 40-km-long fringing coral reef lies off the south shore of Molokai in the Kalohi and Pailolo Channels between Molokai, Lanai, and Maui. The ancestral reef pinches out ~7 km from the west end of the island and 20 km from the east end of the island. The reef flat, a roughly horizontal surface with relatively low coral cover and shore-normal ''ridge-and-runnel'' structures similar to those observed by Blanchon and Jones (1997), typically extends from the shoreline out some distance to the reef crest. The reef crest, where most deep-water waves break, is well defined along most of the reef off southern Molokai and is dominated by encrusting coralline algae, robust lobe, and encrusting corals. Offshore of the reef crest, from depths of 5 m to 30 m, lies the fore reef, the zone of highest coral cover that is generally characterized by shore-normal spur-and-groove structures (Fig. 2).

Data on coral coverage off Molokai were collected during dedicated scuba surveys conducted between February 2000 and February 2002. The four dominant coral species recorded are the delicate finger coral *Porites compressa*, a low-energy species; *Pocillopora meandrina* and *Montipora sp.*, both of which

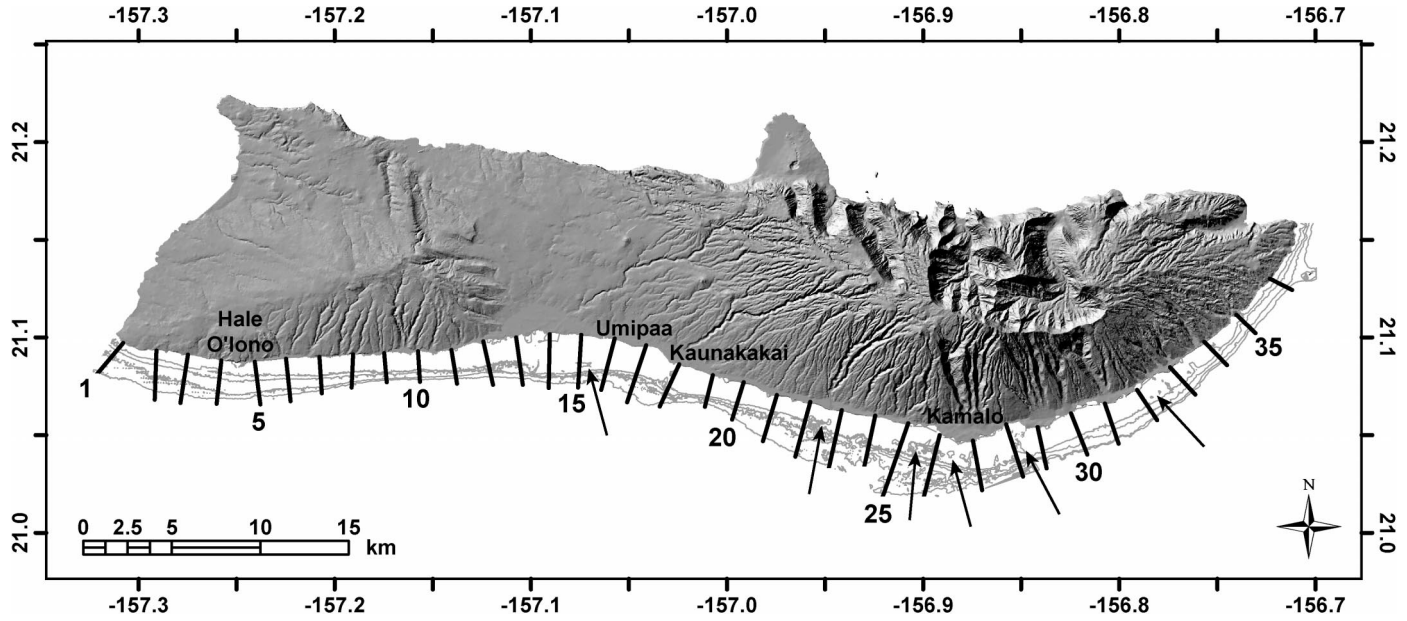

Figure 4. Morphology of the reef and insular shelf off southern Molokai from the SHOALS and National Ocean Service bathymetric data overlaid with the locations of the 36 shore-normal transects used for analysis. The shore-normal transects were spaced roughly every 1.5 km along shore; the isobaths are every 10 m from the shoreline out to 40 m. Arrows denote the location of some prominent "blue holes" on reef flat; note their correlation to onshore drainages.

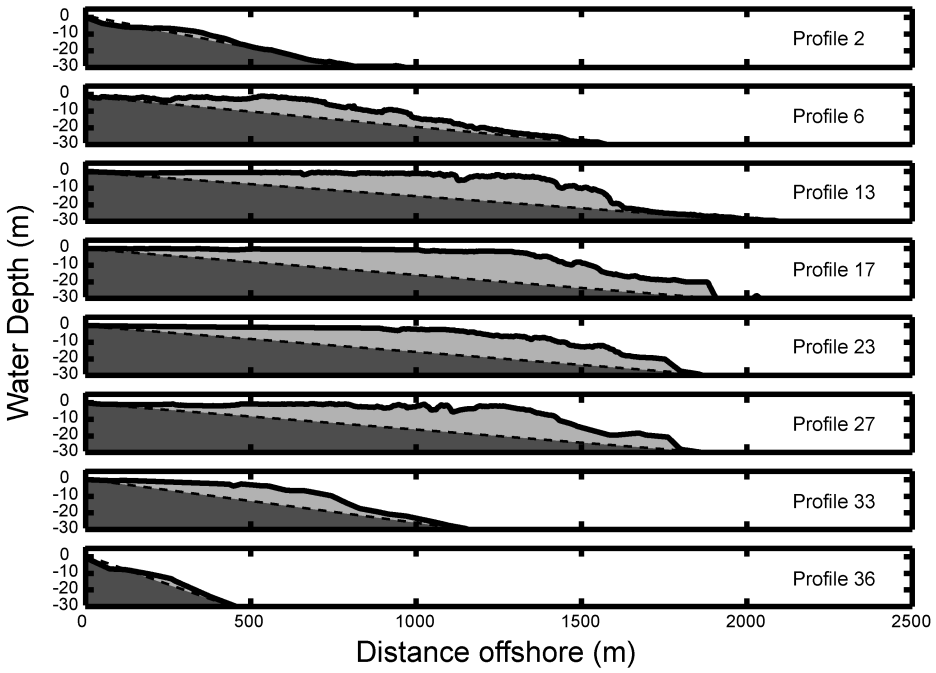

Figure 5. Selected shore-normal reef profiles showing the variation in the development of the reef complex along shore. The dashed lines are a projection of the slopes of the volcanic cone (dark gray) through the reef profiles to provide some insight to the likely cross-sectional area of the reef complex (light gray). Note that the reef is almost nonexistent at the ends of the island (profiles #2 and #36) and extends more than 1500 m offshore of the island's central portion (profiles #13 though #27).

are medium energy and more robust; and *Porites lobata*, a high-energy encrusting or lobate species. The majority of the spurs were primarily covered by the fast-growing *Porites compressa*; the shallower spurs and those in high-energy areas had lower total live coral cover and individually higher percentages of the more robust *P. lobata*, *Montipora sp.*, and *P. meandrina*.

METHODS

Reef Morphology

A digital elevation model of the reef was interpolated from high-resolution bathymetric data collected by the U.S. Army Corps of Engineers SHOALS flights for the USGS in 1999, using geographic information system (GIS) software. The SHOALS system collected ~2,400,000 irregularly spaced laser depth-soundings in overlapping swaths to produce an average horizontal sounding interval of < 3 m. The depth soundings have a vertical accuracy $\pm$ 15 cm and a horizontal accuracy of $\pm$ 3 m. The SHOALS soundings were post-processed to remove spurious data points that may have been caused by environmental factors such as reduced water clarity. The resulting ''clean'' data set consists of X, Y, Z triplets representing individual depth soundings and their locations in Universal Transverse Mercator coordinates. These data were merged

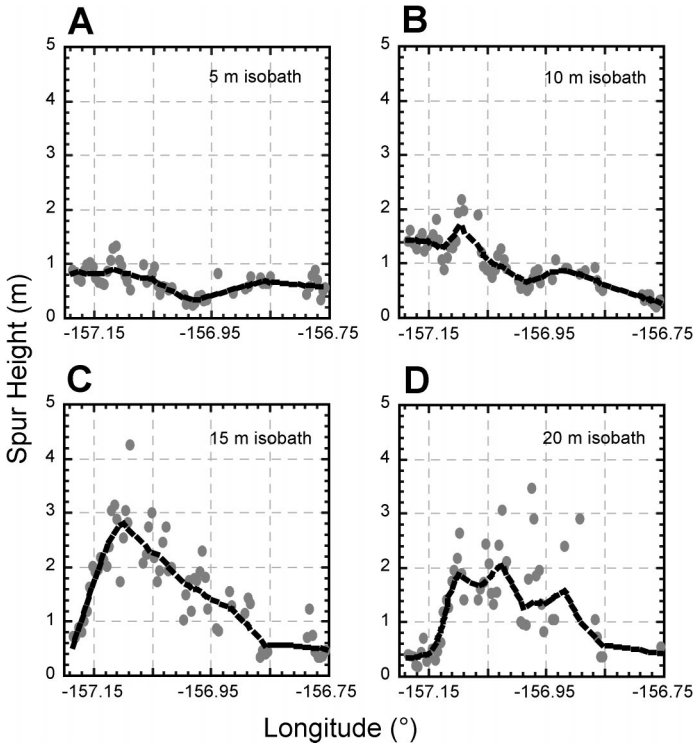

Figure 6. Plots of the spatial distribution of calculated mean spur height along the south shore of Molokai. (A) Along the 5 m isobath. (B) Along the 10 m isobath. (C) Along the 15 m isobath. (D) Along the 20 m isobath. Each of the data points represents the mean spur-and-groove (SAG) height calculated over a 500 m segment of the line. Note that along the 5 m isobath mean spur height is higher near the ends of the island, while at greater depths (15 m – 20 m) the heights are greater near the middle of the island. The dashed curves are 25% running means to display how SAG height tends to vary along shore.

with over 100,000 previously collected U.S. National Ocean Service depth soundings collected along ship tracklines and during harbor surveys. Using these data, a uniform 2 m bathymetric grid was created using the inverse distance-weighting interpolation method based on a 10 m circular neighborhood. The resulting bathymetric surface has a vertical root mean square error of ± 0.09 m when compared to the original SHOALS data.

To quantitatively analyze the reef morphology, multiple shore-normal and shore-parallel bathymetric profiles were derived from the bathymetric grid. The shore-parallel profiles were derived along the general horizontal trend of the isobaths (Fig. 3A). This ensured that the depth variation exhibited in the profiles reflected local morphologic change instead of larger-scale variation caused by the slope of the island. The shore-normal profiles were created roughly every 1.5 km along shore. To facilitate the production of the profile lines, visual aids such as color-shaded relief images, isobaths, and shoreline coverages were incorporated using GIS software. Each profile derived from the bathymetric grid contains geographic coordinates, distance along the specified profile, and water depth at 2 m intervals (Fig. 3B).

Quantitative Morphologic Calculations

Statistics were computed on the position and depth data to define the width of the reef complex and the heights and wavelengths of the spur-and-groove structures. The width of the reef flat was estimated using the arbitrary distance between the shoreline and the 3 m isobath. Three meters was the depth where the break in slope between the reef flat and fore reef could be positively identified in the lidar data and corroborated by numerous field surveys. Field observations suggested that the spur-and-groove wavelengths are never less than 10 m, so the spur-and-groove data were low-pass filtered to remove the high-frequency variations less than 10 m in wavelength. These small features are either small (<9 m^2) sand patches ''pukas'' or large individual coral heads. To make as many calculations of spur-and-groove morphology as possible without including information on larger-scale features such as 'blue holes,' paleo-stream channels, or reentrants, sensitivity analysis was preformed on the spur-and-groove wavelengths. Features larger than 500 m were typically a function of larger-scale structures unrelated to spur-and-groove morphology and thus spur-and-groove height and wavelength were calculated for 500 m segments along each specified isobath. To decrease the degrees of freedom and thus increase confidence in the results, spur-and-groove height and wavelength statistics were computed every 250 m along an isobath, thus using the depth data from 250 m to either side of the point of calculation and creating 50% overlap with each adjacent 500 m section.

After the depth data were low-pass filtered, spur-and-groove heights were computed as the maximum relief between adjacent spur crests and groove troughs and the spur-and-groove wavelength as the distance between adjacent spur crests or groove troughs. Thus, instead of using the spectral methods employed by Roberts et al. (1980), which only provided the mean wavelength and a relative height of the spurs over a specified section of reef, measurements of each individual spur's morphology were made. The heights and wavelengths for each 500 m section were then rounded to the nearest 0.1 m and 1 m, respectively, due to the resolution constraints of the SHOALS data. Each of these histograms was used to calculate the mean and standard deviation of spur-and-groove height and wavelength. If there was a data gap greater than 10% of the segment length (50 m), parameters for that 500 m line segment were not computed.

Wave Data

To provide accurate wave data for locations along the south shore of Molokai, the U.S. Naval Oceanographic Office's Spectral Wave Prediction System (SWAPS) version 4.0 wave model was used. For a detailed description of the SWAPS model, refer to Storlazzi et al. (2002). The model generated a gridded 1.6 km $\times$ 1.6 km field that supplied significant wave height, dominant period, and direction from deep water into the 10 m isobath. Shoaling transformations based on Madsen et al. (1988) theory were made to calculate wave parameters for the specified isobaths.

The wave model results were compared to observations from two U.S. National Oceanic and Atmospheric Administration deep-water buoys (#51001 and #51002) and five pressure

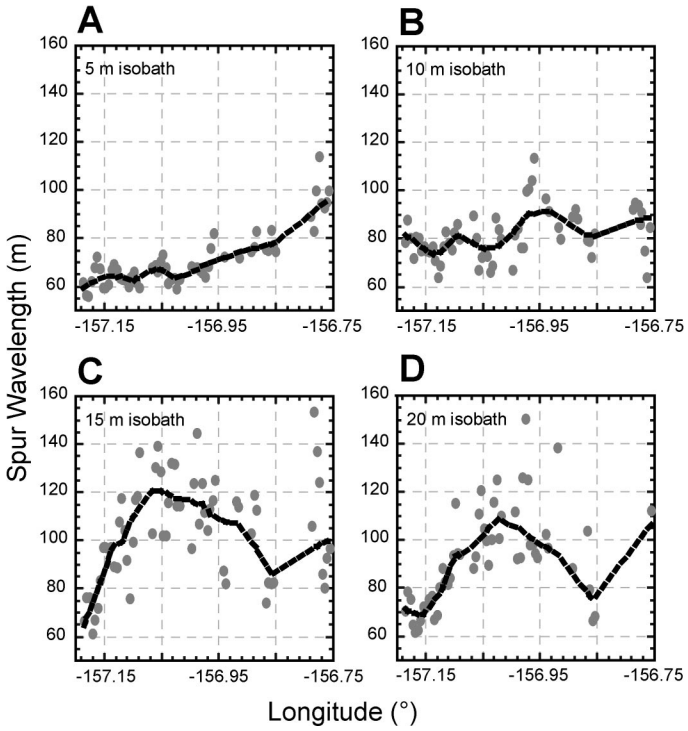

Figure 7. Plots of the spatial distribution of calculated mean spur wavelength along the south shore of Molokai. (A) Along the 5 m isobath. (B) Along the 10 m isobath. (C) Along the 15 m isobath. (D) Along the 20 m isobath. Each of the data points represent the mean spur-and-groove (SAG) wavelength calculated over a 500 m line segment. Note that along the 5 m isobath, and to a lesser extent along the 10 m isobath, mean spur wavelength increases to the island's east end. At greater water depths (15–20 m), spur wavelength tends to be greatest near the island's middle. The dashed curves are 25% running means to display how SAG wavelength tends to vary along shore.

wave gauges we deployed along the 11 m isobath off the south shore of Molokai; both data sets agreed favorably with the wave model output. Since multiple wave conditions impact the coast of Molokai over the course of decades, all of which may be important to reef development, the maximum significant heights and dominant periods that impacted the reef for each grid cell over all wave conditions were employed to reveal the end-member conditions. We then used the H_s and T_p data output by the wave model to calculate the dominant wave horizontal orbital velocity, u, and amplitude excursion, A_e, from linear wave theory. This was then used to calculate both the wave friction factor, f_w (Nielsen, 1992):

$$f_w = 0.04\left[\left(\frac{A_e}{0.0025}\right)^{-0.25}\right] \quad (1)$$

and the peak bed shear stress under oscillatory flow, τ_b (Jonsson, 1966):

$$\sqrt{\tau_b} = \frac{1}{2}\rho_f f_w (A_e\omega)^2 \quad (2)$$

where ρ_f = density of the fluid (kg/m^3) and $\omega = 2\pi/T_p$, radian wave frequency (1/s). These $\sqrt{\tau_b}$ values, in Newtons (N) per m^2, were then compared to reef morphology.

RESULTS

General Morphology

The reef flat is shallow and relatively featureless, attaining a maximum depth of <3 m except in certain locations where ''blue holes'' with nearly vertical walls can extend to depths >35 m (Fig. 4). The reef flat is on average ~1 km wide and has a maximum width of over 1.5 km south of the saddle between the two basaltic shield volcanoes that make up the island. The reef crest is at a nominal depth of 1–2 m and is characterized by more irregular morphology than the reef flat. The fore reef is offshore of the reef crest and extends to depths of 25–30 m where coral cover typically is between 70% and 90%. The morphology of the fore reef is highly variable and is generally characterized by shore-normal spur-and-groove structures or larger-scale features such as paleo-stream channels and reentrants. The reef typically pinches out and intersects the shelf between the 25 m and 30 m isobaths, with hard corals giving way to sand flats dominated by patches of calcareous *Halimeda* algae similar to those observed by Dollar (1982).

Thirty-six shore-normal transects were computed from the shoreline out to the base of the present reef at ~1.5 km intervals along the 30 m isobath off the south shore of Molokai; selected profiles of the reef along these transects are shown in Figure 5. For reference, representations of the volcanic cones' slope through the reef profiles are included to provide some insight to the likely cross-sectional area of the reef complex. Profiles #2 and #36 clearly demonstrate that no shallow reef flat is present at the ends of the island and suggest that these profiles are good examples of the island where no well-defined reef complex exists; field observations showed a very thin veneer of live coral overlying volcanic substrate. Profiles #13–27 display a well-defined reef flat that extends over 1200 m offshore. These profiles also show a steeper slope from greater than 20 m to the 30 m isobath, which corresponds to the toe of the present-day living reef observed during scuba transects, similar to that observed by Dollar (1982). Profiles #6 and #33 show the transition from no clearly defined reef at the ends of the island to the well-defined reef shown off the central portion of the island (Profiles #13–27). These profiles (#6 and #33) display a reef flat that is 500 m wide on average and a less steeply sloping fore reef that lacks the abrupt increase in slope between the 20 m and 30 m isobaths seen in Profiles #13–27.

Spur-and-Groove Morphology

In total, 4791 spur-and-groove structures were mapped from the SHOALS data along the four isobaths, with a range from 1079 to 1386 spur-and-groove structures per isobath. From these data, we computed mean spur height and wavelength at more than 50 overlapping 500 m intervals along ~30 km of the reef. Along the 5 m isobath (Fig. 6A), mean spur-and-groove heights were typically less than 1 m, with the lowest heights calculated in the middle of the reef. Spurs at the 5 m isobath typically have much lower total coral cover than those along deeper portions of the reef. The species that are commonly observed are *P. meandrina* and the more robust *P. lobata*. The along-shore trend at the 10 m isobath was different than at the 5 m isobath,

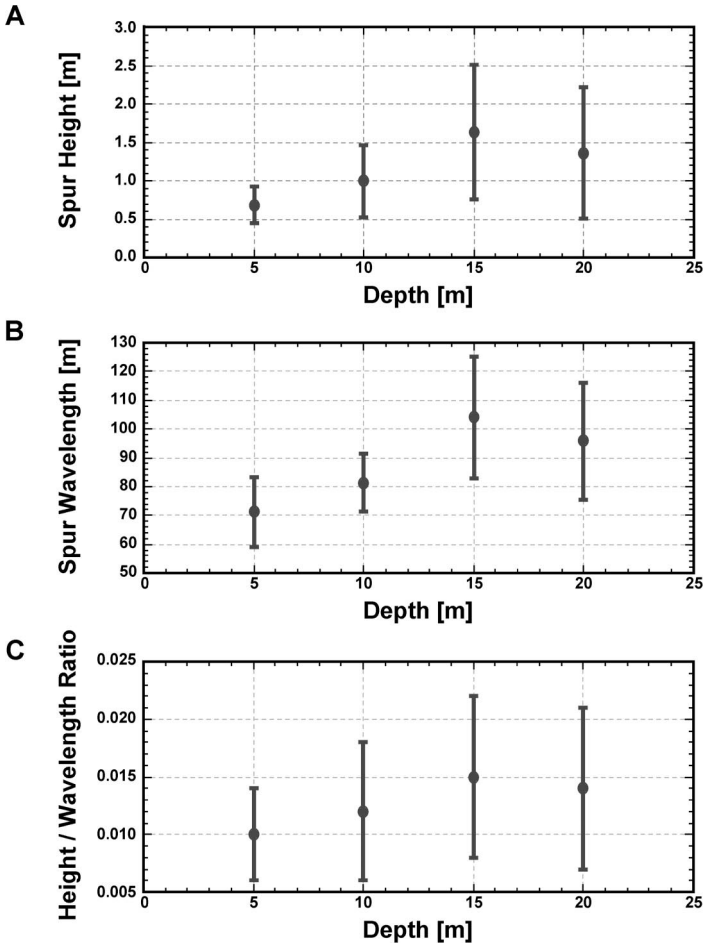

Figure 8. Variation in mean spur-and-groove (SAG) morphology with water depth. (A) Mean ± 1 standard deviation of spur height. (B) Mean ± 1 standard deviation of spur wavelength. (C) Mean ± 1 standard deviation of the ratio of mean spur height to mean spur wavelength with water depth. Note how all three parameters' means and variability are smallest at the 5 m isobath and largest at the 15 m isobath and then slightly less at the 20 m isobath than at the 15 m isobath. These variations are likely a trade-off between light available for photosynthesis and wave energy.

with the lowest mean spur-and-groove heights observed at the east end of the island and a general increase in height from east to west (Fig. 6B). The trends in mean spur-and-groove height observed along the 15 m and 20 m isobaths were opposite those calculated for the 5 m isobath, displaying the greatest heights (> 3 m) in the middle of the island (Fig. 6, C and D). The spurs observed between the 10 m and 20 m isobaths typically have much higher percentages of live coral than those at 5 m. The deeper spurs tend to have slightly lower coral coverage at both the east and west ends of the island where exposure to large waves increases and they are covered by more robust species of coral (*P. lobata* and *P. meandrina*) than along the sheltered central portion of the reef at similar depths where *P. compressa* is dominant.

Two trends were observed in the calculated mean spur-and-groove wavelength values. Mean wavelength along both the 5 m and 10 m isobaths increased toward the east end of the island, with the wavelength being slightly greater on average along the 10 m isobath than the 5 m isobath (Fig. 7, A and B). Mean spur-and-groove wavelengths along the 15 m and 20 m isobaths exhibited a different trend than those observed along the two shallower isobaths, with the largest wavelength values generally observed at the center of the island (Fig. 7, C and D).

On average, the lowest (0.7 m) and least variable mean spur-and-groove heights were observed along the 5 m isobath, whereas the largest (1.6 m) and most variable mean heights were measured along the 15 m isobath (Fig. 8A). Similarly, the longest mean (104 m) and most variable mean spur-and-groove wavelength were calculated for the 15 m isobath, whereas the 5 m isobath displayed on average both the smallest (71 m) and least variable wavelengths (Fig. 8B). The variation in the ratio of spur height to wavelength with depth displayed a pattern similar to spur height and wavelength, increasing from the 5 m isobath to the 15 m isobath, then decreasing slightly from the 15 m isobath to the 20 m isobath (Fig 8C). This trend suggests that spurs tend to become more peaked (greater height to width ratio) with increasing water depth. Overall, field observations showed that the grooves tend to be wider relative to the spur width in shallow water depths (especially in more exposed areas) than in deeper water, where the grooves tend to be narrower.

Wave Energy

The maximum near-bed horizontal wave-orbital velocity component was calculated from the wave model results to better understand the influence of wave-orbital velocities on the reef. The maximum velocities were dominated by the large (6+ m), long-period (22 s) North Pacific winter waves, which generated high (>1.5 m/s) wave orbital velocities and shear stresses (>1.5 N/m^2) along the entire north shore and both the east and west ends of Molokai (Fig. 9). Some wave energy refracts around the west end of the island, resulting in very high orbital velocities along the south shore within a few kilometers of the west end. The rest of the south shore exhibited moderately low (<0.5 N/m^2) peak near-bed stresses. The coastline between the southernmost point of the island at Kamalo and the east end of the island (Fig. 4) is directly exposed to trade wind waves. This resulted in wave-orbital velocities and peak shear stresses being 50–100% higher than to the west of Kamalo, where the coast is protected from direct trade wind wave impact. The short wave-period characteristic of the trade wind waves was reflected in the greater disparity between the peak near-bed shear stresses for the different isobaths east of Kamalo than to the west of Kamalo, where the coastline is not directly impacted by these waves. Southern Ocean swell and Kona storm waves, which suspend large quantities of fine sediment (Storlazzi et al., 2000), imparted relatively low shear stress (<0.3 N/m^2) along the south shore of Molokai.

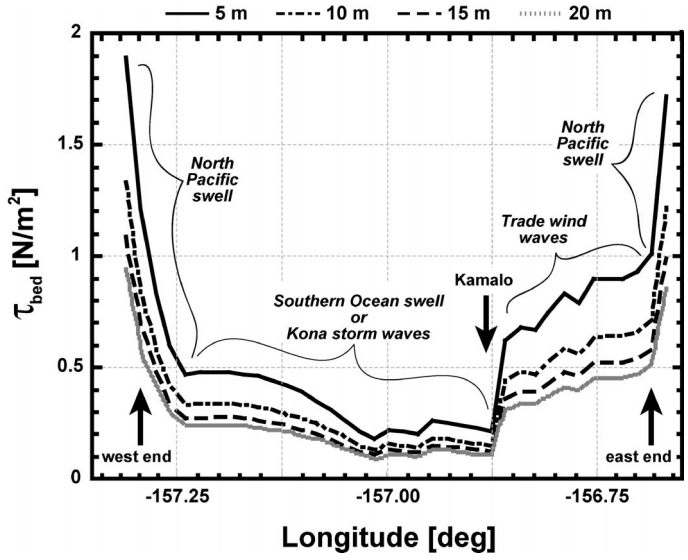

Figure 9. Variation in maximum modeled wave-induced peak bed shear stresses with water depth along the south shore of Molokai and the type of waves responsible for the shear stresses along different sections of the coast. Most of the high stresses associated with the large, long-period North Pacific winter waves typically drop off more than 3 km from the ends of island. The higher modeled stresses east of Kamalo (see Fig. 4 for location) are caused by the open exposure of this section of the reef to trade wind waves, which directly impact this section of shoreline through channel between Molokai and Maui. Most of the remainder of south shore is in the lee of Lanai from Southern Ocean swell or Kona storm waves.

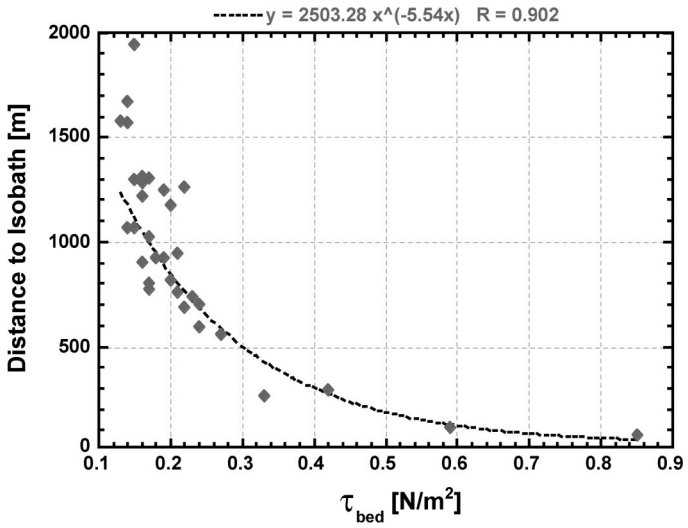

Figure 10. Relationship between reef flat width and modeled wave-induced peak bed shear stresses for all 36 shore-normal profiles. The width of the reef flat is approximated as the distance between the shoreline and the 3 m isobath as determined from the SHOALS data and numerous snorkel transects. The exponential curve fit is significant above the 0.1% level.

Relationships Between Wave Energy and Reef Morphology

A strong inverse exponential relationship ($r^2 > 0.81$) exists between the modeled shear stresses and the width of the reef flat (Fig. 10). This correlation exceeds the 0.1% significance level for $n = 36$ and infers that reef flat width, and thus very likely the overall reef width, decreases exponentially with increasing wave energy.

Computed mean spur heights and wavelengths were compared to the modeled wave-induced peak bed shear stresses to determine if there are any relationships between spur-and-groove morphology and waves. Mean spur height along all four isobaths was shown to decrease logarithmically with increasing modeled near-bed shear stress (Fig. 11A); the significance of this correlation is above the 0.1% level for $n = 89$. Mean spur wavelength along all four isobaths showed a similar relation to wave energy, decreasing logarithmically with increasing peak bed shear stress with significance above the 0.1% level (Fig. 11B). Spur height and wavelengths at shallow depths (5 m), however, both displayed a trend opposite the data for all of the isobaths, with a slight increase in height or wavelength with increasing peak bed shear stress (not shown). The ratio of spur height to wavelength also decreased logarithmically with increasing wave-induced near-bed shear stress (Fig. 11C); this relationship is significant at the 1% level. The low percentages of variability explained by these correlations between waves and spur-and-groove morphology are likely due to a number of factors. These include natural variability in a complex biogeomorphological system, the disproportionate spatial resolutions of the SHOALS data (order of meters) and the wave model output (order of kilometers), and other important controls like variations in light availability for photosynthesis due to turbidity.

Spur-and-groove morphology appeared to occur in two distinctly different groups based on wave energy (Fig. 12). Overall, spur-and-groove structures tended to be more than twice as high (1.1 m) and slightly wider (93 m) in lower-energy environments as those in higher-energy environments (0.5 m and 87 m, respectively). Numerous short, narrow spur-and-groove structures occurred at shallow-water (Fig. 12A) depths, whereas in mid-water depths (Fig. 12B), fewer, broader, and taller spurs dominated, followed by a reversal back to more numerous short and narrow spurs lower on the fore reef along the 20 m isobath. The many short, high-frequency spur-and-

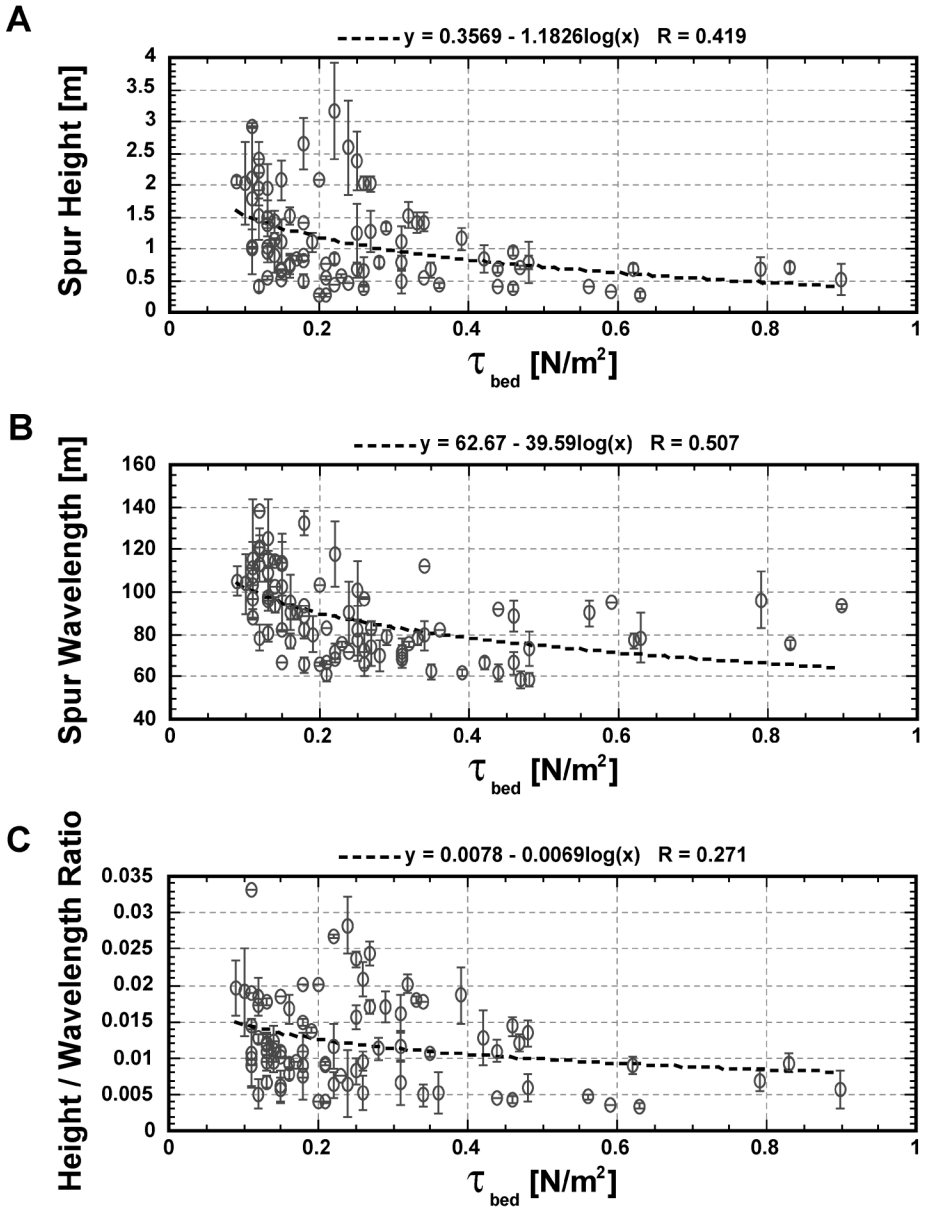

Figure 11. Relationship between spur-and-groove (SAG) morphologic parameters and modeled wave-induced peak bed shear stresses: (A) Mean spur height; (B) mean spur wavelength; and (C) the ratio of mean spur height to mean spur wavelength. Spur height and wavelength are variable but tend to be higher and longer, respectively, at low wave-induced shear stresses and become smaller and shorter, respectively at high shear stresses. Both of these relationships are significant above the 0.1% level while the height to wavelength ratio's relationship is only significant at the 2% level. This high significance suggests waves are the dominant factor controlling SAG morphology while the relatively low percent of variability explained by the curves are likely due to several reasons. Natural system variability and other factors, such as light availability for photosynthesis and turbidity, and the high resolution of SAG measurements as compared to the low spatial resolution of the wave model, are likely sources of variability.

groove structures, either truncated or together, form the less abundant, taller spur-and-groove structures along the 15 m isobath (Fig. 13). The tall, broad spur-and-groove structures deeper on the fore reef typically terminate and are replaced by numerous low mounds or new spurs that are often separated by areas of fine sand from the shallower, continuous spur-and-groove structures. This variation in spur-and-groove morphology causes a change in slope, with a relatively low slope between the 5 m and 15 m isobaths giving way to a steeper slope between the 15 m and 20 m isobaths, forming a morphology similar to the shelf-edge ''buttresses'' observed by Blanchon and Jones (1997).

In higher-energy environments, however, spur-and-groove structures tended to be roughly similar in height and wavelength independent of water depth, with the tallest spurs typically being observed in the shallowest water depths (Fig. 12, C and D). The spur-and-groove measurements in shallow water (5 m) agree with the observations made by Munk and Sargent (1954) along atolls in the western Pacific Ocean and by Roberts (1974) along Grand Cayman in the Caribbean Sea. At greater depths (15–20 m) off Molokai, the spur-and-groove morphology relative to wave energy was the exact opposite of that found by Roberts et al. (1980) and Blanchon and Jones (1997) along the deeper shelf-edge reef off Grand Cayman. The population of reef-forming corals in both the Caribbean and western Pacific is distinctly different from those of Hawaii. It is not clear what role different species may play in influencing the morphology of spur-and-groove structures.

DISCUSSION

The relationships shown here between modeled wave parameters and reef morphology suggest that near-bed, wave-induced shear stresses are a dominant control on the distribution and morphology of the reef off southern Molokai. The central portion of the reef off south-central Molokai is protected from the direct impact by large waves, and thus the reef framework is able to develop into an extensive shallow reef flat and broad fore reef. The east and west ends of the island are exposed to larger, longer period waves that generate high orbital wave velocities and thus strong near-bed shear stresses. This appears to limit substantial reef development because of physical breakage of the coral and high abrasion by both bedload and suspended sediment (Dollar, 1982; Grigg, 1998).

Possible Causes for Variations in Spur-and-Groove Morphology

The primary physical constraints on rocky corals along a single exposed reef are light availability and the forces imposed by fluid flow and abrasion. Both radiant energy, as a percentage of surface illumination, and spec-

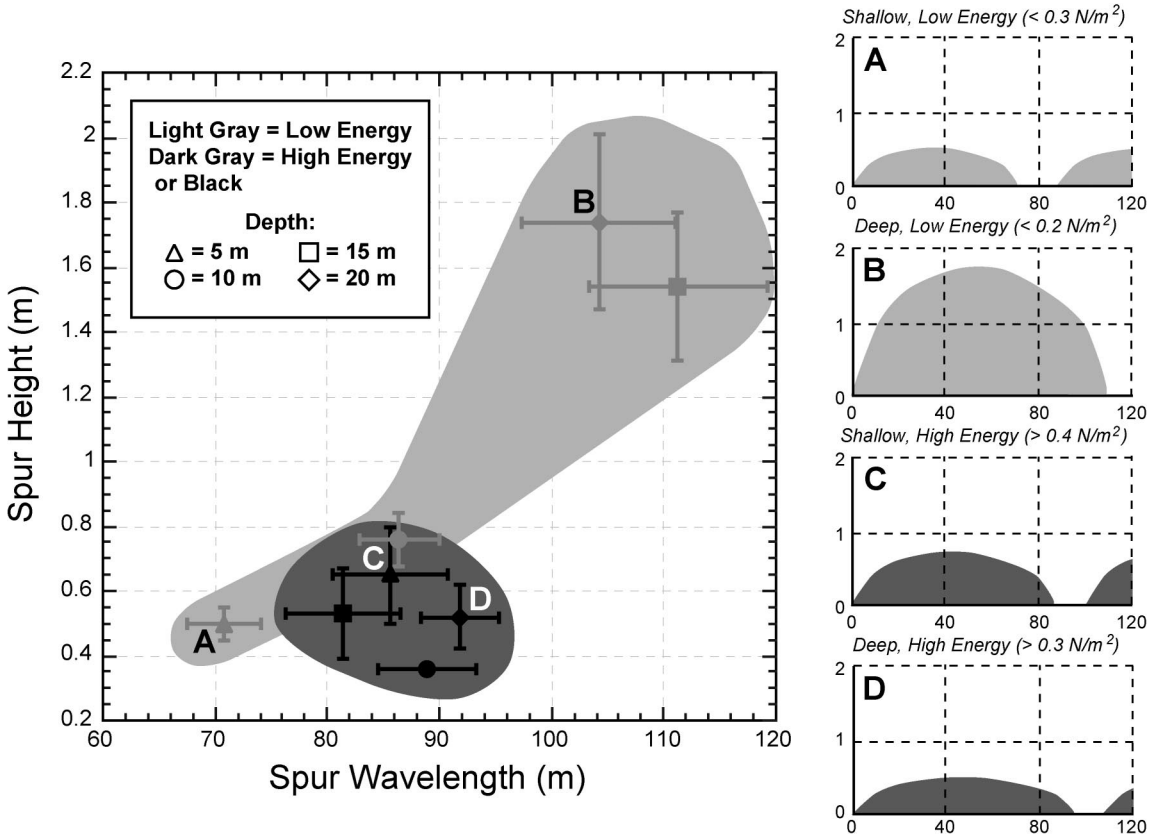

Figure 12. Plot of spur-and-groove (SAG) morphology with respect to wave energy and water depth with schematic cross-section examples of spurs for the different water depths and wave energy end members. (A) Shallow-water, low wave-energy SAG structures. (B) Deep-water, low wave-energy SAG structures. (C) Shallow-water, high wave-energy SAG structures. (D) Deep-water, high wave-energy SAG structures. Note the distinctly different groupings based on wave energy: In low-energy conditions, spurs are small in shallow water and are much larger and broader in deeper water, while spurs in high wave-energy environments display relatively similar morphologies. Deep-water spur heights and widths appear to be dominated by wave-induced forces and in situ coral growth, because spurs in lower-energy environments can grow bigger (up to wave base) and broader. Shallow-water spurs, however, appear to be primarily controlled by binding of broken coral. The higher production of coral rubble and abrasion in shallow, high-energy environments likely promotes coral growth only on high-relief features, causing a positive feedback; diagenetic cementation and algal binding of coral rubble broken by wave-induced forces may also promote taller SAG development in this type of shallow, high-energy environment. Decreased coral breaking, diagenetic cementation, and algal binding in lower-energy, shallow environments would not cause this positive feedback to occur.

tral irradiance have been shown to logarithmically decrease with depth (Stoddart, 1969; Dustan, 1979). These are critical to coral growth because the symbiotic dinoflagellate algae (zooxanthellae) housed in hermatypic corals require light for photosynthesis. Surface wind-wave-induced orbital motions dominate the near-bed flow field on the inner portion (<35 m) of Molokai's insular shelf, where the reef has developed. Wave orbital motions and thus fluid velocities and shear stresses exponentially decrease with increasing depth, as shown by the exponential spacing between the calculated peak bed-shear stresses for each isobath in Figure 9. These motions can, at very high relative stresses, physically break corals, whereas at slightly lower stresses they may inhibit settlement by coral polyps.

The relative heights and wavelengths of spur-and-groove structures provide a proxy of where reef development may be maximized through the combination of high light availability for photosynthesis but relatively low wave-induced shear stress for the species that compose the reef community off southern Molokai (Fig. 8). Maximum calculated mean spur height and wavelength values, and thus spur-and-groove development, were observed along the 15 m isobath. The high light availability in shallower depths (5–10 m) appears to be offset by the high wave-induced shear stresses, keeping spur-and-groove structures small, whereas along the 20 m isobath and deeper, decreased light availability inhibits high relative growth despite the low wave-induced shear stresses (Dollar, 1982).

To explain the variability in spur-and-groove morphology at a given water depth, where light availability remains relatively constant, other physical factors must come into play (Fig. 12). The slightly higher and more widely spaced spurs in higher-energy shallow areas relative to lower-energy regions may be explained by the interaction between sediment and coral. The spurs in the shallow, high-energy portions of the reef are likely constructed, in part, by the binding of coral rubble by diagenetic cementation or coralline algae

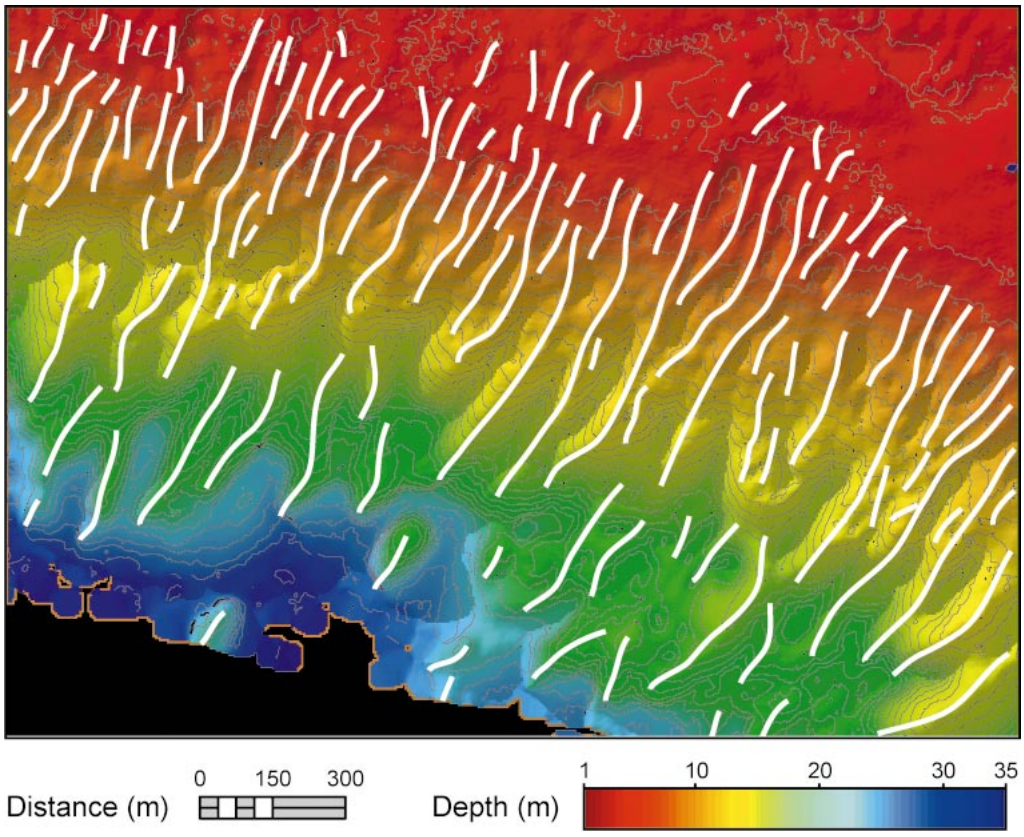

Figure 13. Shaded-height images of the SHOALS bathymetry overlaid with 0.5 m contours to highlight spur-and-groove (SAG) morphology offshore Kaunakakai (see Fig. 4 for location). The white lines denote interpreted spur traces. Note that most of the short, narrow spurs at shallow-water depths merge to form taller, broader spurs around the 15 m isobath. Most of the spurs at the 15 m isobath bifurcate with depth or simply truncate and are replaced by smaller, more closely spaced SAG structures. Some structures around the 20 m isobath are coral-covered mounds isolated by sand from the SAG structures at shallower depths.

as described by Shinn et al. (1981), Macintyre (1997), and Rasser and Riegl (2002). These studies and others (Tribble et al., 1990, 1992; Brainthwaite et al., 2000) have shown that these processes are dominant along low-slope energetic shallow reef crests and upper fore reefs but are absent along the more quiescent deeper portions of the steep fore reef. The large amount of coral rubble and coarse-grained sediment resulting from the weathering of these broken corals may effectively increase the abrasion experienced by lower-lying corals. Consequently, only those spurs with enough height to avoid this abrasion likely promote coral growth. Thus, higher wave energy in more exposed shallow areas may advance spur development through cementation and binding of coral rubble; at depth, higher wave energy may retard intact coral development due to wave stresses where these processes are absent and in-situ coral growth dominates.

Another significant factor shown to control reef development is antecedent topography. While a lower-gradient shelf would result in a greater cross-shore extent of the shelf to be situated in the optimal coral growth zone between light availability and wave energy at any one time, reef development in this space would still be contingent on wave energy weak enough to allow reef growth. This is why well-developed active reefs are not observed off northern Oahu or Maui, regions that have similar coastal configurations but are directly impacted by the large North Pacific swell that generates extremely high (> 1.5 N/m^2) near-bed shear stresses (Grigg, 1998).

These analyses clearly show that waves are the primary control on reef and spur-and-groove morphology where high, wave-induced shear stresses are present. In these areas, light, water depth, and antecedent topography are subordinate. The higher morphologic variability at lower shear stresses demonstrates that when wave-induced water motions are low enough as to not dominate reef and spur-and-groove morphology, other factors such as light availability for in-situ coral growth and the ability to bind or cement rubble increase and may become the dominant factor.

CONCLUSIONS

The application of geodetic-quality airborne lidar bathymetric surveys is very useful for mapping coral reef structures in clear, shallow water. The high water clarity off southern Molokai, Hawaii, allowed mapping of more than 40 km of reef in water depths greater than 35 m. The large quantity of high-resolution bathymetric data makes it possible to perform large-scale quantitative analyses of coral reef morphology. Nearly 5000 morphologic measurements made on spur-and-groove structures provide details on how their structures vary both with water depth and with modeled wave-induced peak near-bed shear stress. Although a number of factors play into coral growth and distribution, the data presented here suggest that the interplay between near-bed shear stress and light availability may be

the prime controls on spur-and-groove morphology along the reef off southern Molokai.

ACKNOWLEDGMENTS

This work was carried out as part of the U.S. Geological Survey Coastal and Marine Geology Program's Coral Reef Project as part of an effort in the United States and its trust territories to better understand the geologic processes that affect coral reef systems. The U.S. Army Corps of Engineers conducted the SHOALS surveys and all of the data processing through an interagency agreement with the USGS. Pat Chavez, Stuart Sides, and Miguel Velasco helped to coordinate the surveys and conducted further post-processing of the data. They, along with Paul Jokiel and Eric Brown, graciously provided insight, friendship, and enthusiasm that contributed substantially to the goals of this paper. We especially thank Captain Joe Reich, who piloted and navigated during the coral coverage surveys and numerous dive transects and instrument deployments. We also thank Jim Gardner and Bruce Richmond, who provided very constructive initial reviews of this manuscript. Use of trademark names does not imply USGS endorsement of products.

REFERENCES CITED

Blanchon, P., and Jones, B., 1995, Marine-planation terraces on the shelf around Grand Cayman: A result of stepped Holocene sea-level rise: Journal of Coastal Research, v. 11, p. 1–33.

Blanchon, P., and Jones, B., 1997, Hurricane control on shelf-edge-reef architecture around Grand Cayman: Sedimentology, v. 44, p. 479–506.

Brainthwaite, C.J.R., Montaggioni, L.F., Camoin, G.F., Dalmasso, H., Dullo, W.C., and Mangini, A., 2000, Origin and development of Holocene coral reefs: A revisited model based on reef boreholes in the Seychelles, Indian Ocean: International Journal of Earth Science, v. 89, p. 431–445.

Clague, D.A., and Dalrymple, G.B., 1989, Tectonics, geochronology, and origin of the Hawaiian–Emperor volcanic chain, *in* Winterer, E.L., Hussong, D. M., and Decker, R.W., eds., The eastern Pacific Ocean and Hawaii: Boulder, Colorado, Geological Society of America, Geology of North America, v. N., p. 188–217.

Cloud, P.E., 1959, Geology of Saipan, Mariana Islands, Part 4—Submarine topography and shallow-water ecology: U.S. Geological Survey Professional Paper 280-K, p. 361–445.

Dollar, S.J., 1982, Wave stress and coral community structure in Hawai'i: Coral Reefs, v. 1, p. 71–81.

Dustan, P., 1979, Distribution of zooxanthellae and photosynthetic chloroplast pigments of the reef-building coral *Monastera annularis*, Ellis and Solander, in relation to depth on a West Indian reef: Bulletin of Marine Science, v. 29, p. 79–95.

Emery, K.O., Tracy, J.I., and Ladd, L.S., 1949, Submarine geology and topography in the northern Marshall Islands: Eos, Transactions of the American Geophysical Union, v. 30, p. 55–58.

Geister, J., 1977, The influence of wave exposure on the ecological zonation of Caribbean coral reefs: Miami, Florida, Proceedings of the Third International Coral Reef Symposium, v. 1, p. 23–29.

Goreau, T.F., 1959, The ecology of Jamaican coral reefs, 1—Species composition and zonation: Ecology, v. 40, p. 67–90.

Grigg, R.W., 1998, Holocene coral reef accretion in Hawaii: A function of wave exposure and sea level history: Coral Reefs, v. 17, p. 263–272.

Jonsson, I.G., 1966, Wave boundary layers and friction factors: Tokyo, Proceedings of the 10th International Conference on Coastal Engineering, p. 127–148.

Kan, H., Hori, N., and Ichikawa, K., 1997, Formation of a coral reef-front spur: Coral Reefs, v. 16, p. 3–4.

Macintyre, I.G., 1997, Reevaluating the role of crustose coraline algae in the construction of coral reefs: Panama City, Panama, Proceedings of the Eighth International Coral Reef Symposium, v. 1, p. 725–730.

Madsen, O.S., Poon, Y.-K., and Graber, H.C., 1988, Spectral wave attenuation by bottom friction: Theory: Proceedings of the 21st Coastal Engineering Conference, American Society of Civil Engineers, v. 2, p. 420–429.

Moberly, R.M., and Chaimberlain, T., 1964, Hawaiian beach systems: Honolulu, University of Hawaii, 95 p.

Munk, W.H., and Sargent, M.C., 1954, Adjustment of Bikini Atoll to ocean waves: U.S. Geological Survey Professional Paper 260-C, p. 275–280.

Nielsen, P., 1992, Coastal bottom boundary layers and sediment transport: Singapore, World Scientific, 324 p.

Rasser, M.W., and Riegl, B., 2002, Holocene coral reef rubble and its binding agents: Coral Reefs, v. 21, p. 57–72.

Roberts, H.H., 1974, Variability of reefs with regard to changes in wave power around an island: Brisbane, Australia, Proceedings of the Second International Coral Reef Symposium, v. 2, p. 497–512.

Roberts, H.H., Murray, S.P., and Suhayda, J.N., 1980, Physical process in a fringing reef system: Journal of Marine Research, v. 33, p. 233–260.

Shinn, E.A., 1963, Spur and groove formation on the Florida reef tract: Journal of Sedimentary Petrology, v. 33, p. 291–303.

Shinn, E.A., Hudson, J.H., Halley, R.B., and Lidz, B., 1977, Topographic control and accumulation rates of some Holocene coral reefs: South Florida and Dry Tortugas: Miami, Florida, Proceedings of the Third International Coral Reef Symposium, v. 1, p. 23–29.

Shinn, E.A., Hudson, J.H., Robbin, D.M., and Lidz, B., 1981, Spurs and grooves revisited: Construction versus erosion, Looe Key Reef, Florida: Miami, Florida, Proceedings of the Fourth International Coral Reef Symposium, v. 1, p. 475–483.

Sneh, A., and Friedman, G.M., 1980, Spur and groove patterns on the reefs of the northern gulf of the Red Sea: Journal of Sedimentary Petrology, v. 50, p. 981–986.

State of Hawaii, 2001, Map of median annual rainfall in millimeters and inches: Molokai, Hawaii, Department of Land and Natural Resources, Electronic data (http://www.state.hi.us/dbedt/gis/).

Stoddart, D.R., 1969, Ecology and morphology of recent coral reefs: Biology Review, v. 44, p. 433–498.

Storlazzi, C.D., Field, M.E., Dykes, J.D., and Ogston, A.S., 2000, Wave control on fringing reef architecture and physical processes: Southern Molokai, Hawaii (abs.): Eos (Transactions, American Geophysical Union), v. 81, p. 683.

Storlazzi, C.D., Field, M.E., Dykes, J.D., Jokiel, P.L., and Brown, E., 2002, Wave control on reef morphology and coral distribution: Molokai, Hawaii, *in* WAVES 2001 Conference Proceedings, San Francisco, California: San Francisco American Society of Civil Engineers, v. 1, p. 784–793.

Tribble, G.W., Sansone, F.J., and Smith, S.V., 1990, Stoichiometric modeling of carbon diagenesis within a coral framework: Geochimica Cosmochimica Acta, v. 54, p. 2439–2449.

Tribble, G.W., Sansone, F.J., Buddemeier, R.W., and Li, Y.-U., 1992, Hydraulic exchange between a coral reef and surface seawater: Geological Society of America Bulletin, v. 104, p. 1280–1291.

Weydert, P., 1979, Direction of growth of the spurs on an outer barrier reef tract_The example of the Grand Récif of Tuléar (Madagascar): Marine Geology, v. 30, p. 9–19.

MANUSCRIPT RECEIVED BY THE SOCIETY 21 JUNE 2002
REVISED MANUSCRIPT RECEIVED 11 MARCH 2003
MANUSCRIPT ACCEPTED 6 MAY 2003

Printed in the USA